

# Extensional rupture of model non-Newtonian fluid filaments

Joel Koplik

*Benjamin Levich Institute and Department of Physics,  
City College of the City University of New York, New York, NY 10031*

Jayanth R. Banavar

*Department of Physics, The Pennsylvania State University, University Park, PA 16802  
(February 1, 2008)*

We present molecular dynamics computer simulations of filaments of model non-Newtonian liquid stretched in a uniaxial deformation to the point of breaking. The liquid consists of Lennard-Jones monomers bound into chains of 100 monomers by nonlinear springs, and several different constant velocity and constant strain rate deformations are considered. Generally we observe nonuniform extensions originating in an interplay between the stretching forces and elastic and capillary restoring mechanisms, leading to highly uneven shapes and alternating stretched and unstretched regions of liquid. Except at the fastest pulling speeds, the filaments continue to thin indefinitely and break only when depleted of molecules, rather than common viscoelastic rupture mechanisms.

PACS numbers: 83.50.-v, 61.25.Hq, 47.55.Dz, 47.20.Dr

## I. INTRODUCTION

The extensional dynamics of polymeric, non-Newtonian liquids controls processes ranging from commonplace activities such as chewing gum to large-scale commercial applications in extrusion processing of materials [1]. Understanding the dynamics of the liquid in these situations [2] requires information beyond the usual shear viscosity characterization of flowing fluids, and has led to extensive experimental and theoretical work on “liquid bridges” [3]. Here, one pulls on the ends of a cylinder of the liquid and observes shapes, forces, velocities and (to some degree) stresses, and attempts to relate the behavior to an appropriate rheological model. The ultimate fate of an extending liquid bridge is a rupture at some point, and one component of the efforts in this subject has attempted to understand the fracture mechanisms involved. Aside from practical relevance to materials failure, the thinning dynamics of a cylindrical neck of liquid has become an important subject in fluid interfacial dynamics [4]. In almost all cases, these efforts have concerned macroscopic bodies of liquid, in the sense that the experiments do not generally have atomic resolution, and the calculations are based on continuum descriptions. The purpose of this paper is to consider the interfacial rupture of a liquid bridge configuration at an atomic scale. In addition to the intellectual question of exploring the late stages of rupture that are below the level of resolution considered previously, a further motivation comes from recent interest in micro- and nano-fluidics [5], where precisely these length and time scales can be reached in practice.

The focus of this paper is somewhat outside the issues usually considered in rheology. Previous studies of the rupture of liquid filaments [6] have concentrated on determining instability criteria based on continuum modeling. The focus has been on constant strain-rate deformations, and on identifying characteristic regions of the strain rate – maximum strain phase space, corresponding to viscous, elastic, rubbery and glassy behavior. It has proven useful to distinguish a recoverable component of the strain, representing the residual deformation of the material when the stretching forces are released and it is allowed to retract (i.e., omitting viscous flow deformations). It is inferred that true rupture occurs only when this recoverable strain exceeds 1/2. In the systems studied here, the chain molecules can distort in shape but not divide or combine, but one possible mechanism for a nonrecoverable strain could involve permanent disentanglement of the chains. A second focus of previous work has been the relation between time to rupture and applied stress; in our simulations the ends of the filament are moved at prescribed velocities, so that applied stress is not fixed and instead fluctuates during the course of the stretch. To discuss other configurations, empirical correlations or the results of non-Newtonian continuum modeling are used. The simulations performed here quickly lead to regions of filament which are only a few molecules in diameter, and not obviously described in these ways.

We have previously considered the rupture of fluid interfaces in two situations, using molecular dynamics (MD) simulations. In a study of the dynamics of a monatomic drop placed in an second immiscible fluid undergoing shear [7], we found fair quantitative agreement with experiments and continuum calculations in general, and in particular that the drop ruptures at a sufficiently large capillary number. The microscopic mechanism involved is a gradual flow of the drop’s molecules to one side or another induced by the external flow, coupled to surface tension (originating in the molecular interactions chosen to provide immiscibility) acting to reduce the area of the interface separating the

drop and solvent liquids. In a previous paper on non-Newtonian fluids [9] we used MD simulations to study liquid bridge deformation, focusing on the shape evolution and internal velocity and stress fields. In that paper relatively small samples of several different model molecular fluids were considered – a Newtonian liquid based on short chain molecules, a solution of a few longer (20-40 monomer) molecules in a short-chain solvent, and melts of the longer chains. Although the simulations were continued to the point of rupture, these systems were too small to display any interesting behavior in that regard which could be quantitatively analyzed. The Newtonian liquid and melt systems ruptured due to fracture after only modest length increases, by less than a factor of two. The model solution system attained rather longer lengths, by virtue of the longer molecules becoming extended and providing a kind of backbone, and ruptured when the overall length exceeded the amount of molecular backbone available, essentially following the monatomic mechanism. Our goal here is to use a larger system based on a melt of longer molecules, and study the deformations of highly elongated liquid filaments.

## II. SIMULATION PROCEDURE

The simulational method and the molecular system closely follows our earlier papers on nanodrop dynamics [8], liquid bridge extensional flows [9], and single chains in a flow [10]. The MD calculations themselves are of standard form [11,12], and consider a fluid made of monomers interacting with two-body forces of two types, a Lennard-Jones potential to provide an impenetrable core and chemical attraction at larger distances, along with a finitely-extensible nonlinear elastic force to link the monomers into model polymer chains. The explicit forms of the interaction potentials are

$$V_{\text{LJ}}(r) = 4\epsilon \left[ \left( \frac{r}{\sigma} \right)^{-12} - \left( \frac{r}{\sigma} \right)^{-6} \right] \quad V_{\text{FENE}}(r) = \frac{1}{2}kr_0^2 \ln \left( 1 - \frac{r^2}{r_0^2} \right) \quad (1)$$

The Lennard-Jones interaction acts between any two monomers separated by a distance less than  $r_c = 2.5\sigma$ , and a linear term is added to  $V_{\text{LJ}}$  so that the force vanishes at this cutoff. The FENE potential [2] acts only between adjoining monomers in any one molecule, and has the effect of limiting the bond length to  $r_0$ . The parameters in the FENE potential are taken to be  $r_0 = 1.5\sigma$  and  $k = 30\epsilon/\sigma^2$ , following Kremer and Grest [13], and are chosen to yield an entangled melt of non-crossing chains for the 100-monomer chain length used here. The characteristic time for monomer dynamics is defined by the LJ parameters,  $\tau = \sqrt{\epsilon/m\sigma^2}$ , where  $m$  is the monomer mass. In the remainder of this paper, and in particular in all figures, when dimensions are not given we are implicitly using “MD units” where  $\sigma$  is the unit of length,  $\tau$  is the unit of time, and  $\epsilon$  the unit of energy.

A molecular liquid based on the FENE and LJ potentials (1) has been widely studied as an MD a model of polymer melts [14]. In most previous work, the 6-12 potential is cut off at a smaller value than used here,  $r_c = 2^{1/6}\sigma$ , which has the computational advantage of reducing the number of particles which are in interaction range, and speeding the calculation. The properties of this system are given in detail in [15]. This value of  $r_c$  corresponds to a purely repulsive potential which, while adequate for a confined material, has the disadvantage here that a fluid will expand to fill space uniformly, with no interface. Since an interface is crucial here, attraction is needed and we retain the larger value of  $r_c$ . However, because the interaction has been altered, the liquid studied here need not have the same transport coefficients. In separate simulations we find a static shear viscosity  $\mu(0) \sim 10^3 m/\sigma\tau$ , defined as the limit of the dynamic shear viscosity  $\mu(\dot{\gamma})$ , the ratio of shear stress to strain rate in Couette flow, when the strain rate tends to zero. Typically polymer melts based on LJ and FENE potentials show shear thinning – a nearly constant viscosity up to a certain transition shear rate  $\dot{\gamma}^*$ , and a systematic (roughly power-law) decrease at larger values. We use the inverse of the transition shear rate as a characteristic fluid relaxation time,  $\lambda \equiv 1/\dot{\gamma}^* \sim 10^5 \tau$ , in this case. This number and the quoted viscosity above are very crude estimates: at the very low velocities needed to reach the plateau for this chain length, the signal-to-noise ratio in a stress measurement is poor, and even in very long runs substantial fluctuations are found. The rheology of chain liquids and the definition of characteristic time in this context is discussed further in [15,9]; the latter paper considers MD simulations of the liquid bridge extensional dynamics of model melts (and other fluids) and also shows that they exhibit strain-hardening in extensional flow, in the sense that an appropriate extensional viscosity increases with strain rate. Lastly, the surface tension is measured to be  $\alpha = 0.37 \pm 0.01$  using an independent equilibrium simulation of a slab of liquid with planar interfaces [16].

The MD calculations are performed in parallel on either T-3E, Origin-3000 or IBM SP platforms, using a spatial domain decomposition algorithm, a layered linked-cell list on each processor, and MPI routines. The numerical procedure is to integrate Newton’s equations of motion using the velocity Verlet algorithm [11] with time step  $0.005\tau$ . Occasionally the computation was checked by re-running over a certain time interval with a smaller step length. A Nosé-Hoover thermostat [17] is used to maintain the liquid at a constant temperature  $T = 1.5\epsilon/k_B$ . The initial configuration, a roughly-circular cylinder of length  $L_0 = 80.5\sigma$  and radius  $R_0 = 26.3\sigma$ , containing 1400 chain molecules

100 monomers in length, is in a disordered liquid state resulting from a somewhat convoluted preparation procedure. In our earlier simulations of length-100 chain molecule melts [8], we began with the monomers on regular lattice sites and randomized the configuration by cooking it at a high temperature and low density in a box with repulsive walls. This system was equilibrated to the point where its time-averaged monomer spatial density was uniform, the probability distributions of molecular sizes (end-to-end length and radius of gyration) reached a steady state, and the probability distributions of molecular orientations were rotationally invariant. A spherical drop was formed by cooling the liquid gradually to temperature 1.5, while simultaneously applying a weak central force until a stable sphere formed, and then gradually switching off the force. Next, half of the sphere was placed on a partially-wetting atomistic solid substrate and re-equilibrated, and finally the sphere was allowed to coalesce with a slightly randomized copy of itself. Because both hemispheres were placed on attracting substrates, the result was a liquid cylinder held between two solid surfaces, rather than a single larger sphere. Removing the solid substrate after coalescence gives the initial cylinder considered here. One might be concerned that when the cylinder is pulled it would tend to break at the mid-plane into its two original drops due to incomplete healing, but in fact we observe rupture at various other locations.

To stretch the filament, we simply pull on its ends. More precisely, each monomer in a disk of thickness  $5\sigma$  at each end is attached to a “tether site” by a stiff spring, and the tethers are moved outwards in a prescribed manner by displacing their position by the appropriate axial amount  $\pm v_0\Delta t \hat{z}$  at each time step. In simulations of constant-velocity extension,  $v_0$  is just the velocities at each end of the filament, while for constant-strain-rate extension where the length of the filament grows as  $L(t) = L_0 e^{\dot{\epsilon}_0 t}$ , the fixed control parameter is the strain rate  $\dot{\epsilon}_0$ , and the velocity is  $v_0(t) = dL(t)/dt$ . This procedure is similar to a common experimental one [3] where the liquid filament rests between solid end plates which are moved apart, but has the conveniences that the end plates need not be modeled and that flow along the end plates does not arise. The focus of this paper is the behavior of the liquid in the “middle” of the filament, so nothing is lost in this way. We also attempted an alternative procedure suggested by experiments on single DNA molecules [18] in which a constant axial force was applied to each monomer in the end regions, but the result was that the end regions contracted radially and ruptured occurred nearby, leaving the bulk of the filament unextended.

The operating conditions of the various simulations performed here are listed in Table I, in terms of the pulling velocity or strain rate. Note that in either case the initial velocity and strain rate are related by  $v_0 = L_0 \dot{\epsilon}_0$ , where  $L_0$  is the filament’s initial length. In terms of the usual dimensionless groups characterizing a flow, at the start of a run the Reynolds number  $Re = \rho v_0 R_0 / \mu(0)$  is always much less than unity, while the Deborah number  $De = \lambda \dot{\epsilon}_0$  and the capillary number  $Ca = \mu(0)v_0/\alpha$  are  $O(10^2)$  or larger. Although the Reynolds, Deborah and capillary numbers describing this flow are all moderate by laboratory standards, it should be kept in mind that the physical velocities are relatively large, meters to hundreds of meters per second (depending on one’s interpretation of the Lennard-Jones monomers), and not at all small for the microscopically thin bodies of liquid considered here.

### III. CONSTANT VELOCITY STRETCHING

We first consider filament stretching at a relatively low constant velocity, displacing the two ends at  $\pm 0.05\sigma/\tau$ . Successive snapshots of the filament appear in Fig. 1, in a low-resolution side view intended to indicate the overall shape. At early times there is a mostly-uniform deformation, aside from some necking near the two ends which results from the tethering method used here – the monomers there are essentially pinned to their initial relative positions and when these are moved apart the melt attempts to fill in. A “dynamical” necking down appears near the center of the filament around  $1500\tau$ , followed by relatively uniform stretching of the central neck region through  $3100\tau$ , while the two end segments of the filament translate with the tethers with only minor changes of shape. Eventually the filament breaks when the neck region is so stretched as to run out of molecules. As seen in the close-up views in Fig. 2, the neck eventually thins down to a few molecular chains lined up along the stretch axis, and the breakage occurs when these chains are pulled in opposite direction and slide past each other. Note that the molecular model used here does not incorporate chain breaking, so the molecular “depletion” seen here is the only available rupture mechanism.

Calculations and laboratory experiments [4,19,20] on the thinning of a continuum Newtonian liquid cylinder typically find a power-law variation of minimum radius with time. Here, however, while we do observe a systematic decrease as seen in Fig. 3, the detailed time variation is not well fit by a power of time. Aside from the fact that the later stages of rupture are associated with a neck made of just a small number of highly extended molecules, it is not unreasonable to see quantitatively different behavior. Furthermore, at this stage the liquid is presumably highly viscoelastic so that Newtonian fluid predictions may not be applicable. Similar behavior is observed in all of the other cases presented below: although there is a systematic decrease in the filaments’ minimum radius with time, it does not fit a power-law variation. Figures 8 and 9 show a sequence of snapshots at higher (fixed) tether speeds,  $\pm 0.15$

and  $\pm 0.5\sigma/\tau$  respectively. In these various simulations, the initial liquid cylinder is always the same, and within each sequence the same length scale is used. First note that the rupture occurs at different points along the filament, indicating that the process is random and an indirect function of the particular sequence of fluctuating positions and velocities in each case, and furthermore that there is no special defect associated with the “sample preparation”. At these higher speeds, the stagnant end regions at the ends do not develop, and more molecules are available to the central portion of the filament, allowing it to attain longer strains before rupture. Here the ends are steadily drawn out, leaving a central region which does expand but at a distinctly slower speed, and begins to evolve into isolated drops. In the central region, relatively rapid thinning occurs at several intermediate points, and the configuration prior to rupture resembles the results of the quasi-static Rayleigh instability [7], where a cylinder of liquid without imposed flow breaks up into spherical drops. The final stages of rupture, again, amount to a very narrow neck only a few molecules in width attenuating down to nothing as its elongated chains are pulled past each other. The shape evolution is in a sense opposite to that of the low-velocity case in Fig. 1, where the end regions began to translate passively before becoming highly stretched. Finally, as indicated in Table I, note that the maximum length attained before breakup increases with pulling speed while the time to rupture decreases, presumably because the higher stress allows more molecules to be stretched.

#### IV. CONSTANT STRAIN RATE STRETCHING

The more common experimental protocol in liquid bridge systems is stretching at constant strain rate,  $\dot{\epsilon}_0 = \dot{L}(t)/L(t)$ , leading to an exponential increase in length and velocity. Ostensibly the motivation is to provide a constant “strain environment” for the liquid, to facilitate study of its extensional rheology, although in practice [3,9] the strain can often be very unevenly distributed. In Fig. 10 we show some of the time-sequence of shapes observed at a strain rate  $\dot{\epsilon}_0 = 0.001\tau^{-1}$ . The evolution combines features of the various constant-velocity deformations presented above: the filament narrows in the center and eventually ruptures there due to attenuation of molecules, but at the same time the end regions are not translating stagnantly but rather stretch at a slower rate than the bulk, and at the time of rupture are themselves in the process of thinning and presumably would eventually break up due to the Rayleigh instability.

The distinction between constant-velocity and constant-strain deformations is that in the former case the strain rate (and stress) decrease with time, so that after an initial stage where the system is pulled out of its equilibrium configuration, the molecules can relax back; see Fig. 4. In the present case, the stress is ostensibly constant, and the molecules are increasingly elongated and oriented with no configurational relaxation until nearly the time of rupture, as shown in Fig. 11. The behavior of the velocity profiles is also consistent with these remarks; as seen in Fig. 12, the velocity is closer to a linear variation along the axis for a considerably longer time interval.

A somewhat related MD study [21] of the elongation and relaxation of a model polymer melt considered chains of 30 monomers using the same interactions as in this paper (but with a short  $r_c = 2^{1/6}\sigma$  LJ cutoff). Instead of simulating the explicit stretching of filaments, a nonequilibrium MD method was used to apply a constant-strain uniaxial elongation to a homogeneous system in a box. Among other things, the behavior of the chain size (radius of gyration) and orientation was measured, and the qualitative behavior is similar to that seen here. The elongation and degree of orientation increased monotonically during the flow, at a rate which increased monotonically with the strain rate, and then relaxed monotonically when the flow was turned off.

We have considered the question of unrecoverable strain [6] in this simulation, by releasing the tethered monomers and allowing the liquid to take up a new equilibrium shape without external stress. If the filament is released well before rupture, it seems to withdraw into a sphere, whereas if released just before rupture the thinning neck continues to thin, rupture occurs anyway, and afterwards the liquid appears to be withdrawing into two spheres. Here the phrase “appears to be” means that as a function of time the liquid shape is tending towards one or two spheres at the original liquid density, but the process is so slow that we have not followed it all the way to equilibrium. The asymptotic strain does, however, go well below 1/2, and we do not see the values of unrecoverable strain suggested in [6]. Similar behavior is found in the other cases as well. Given that the initial simulated filament was prepared by an equilibration procedure involving relaxation of a dilute high-temperature melt, it is difficult to see how the final state here would differ in any statistically significant way, other than perhaps the time needed to reach it.

At higher strain rates a different behavior appears, a cohesive failure of the melt in the region where the molecules are tethered to pulling sites. In Fig. 13, at strain rate  $\dot{\epsilon}_0 = 0.004$ , there is a rapid thinning at the ends of the filament leaving a central stagnant region showing the onset of a Rayleigh instability, while the thin necks attaching this region to the ends attenuate until breakup. At the same time, some of the tethered molecules are pulled out of the filament, and the fluid bodies at the ends have not had time to relax to an equilibrium shape. At the still higher strain rate  $\dot{\epsilon}_0 = 0.01$  shown in Fig. 14, the tethered molecules are simply pulled free of rest of the the filament, and rapid rupture

occurs. The rupture times and lengths for the various cases are recorded in Table I.

## V. FORCE MEASUREMENTS

As an alternative to the stress fields, we have studied the forces from a more direct viewpoint on the monomer scale. The quantity of perhaps most direct experimental relevance is the pulling force exerted on the tethers at the ends. While this quantity is easy to evaluate in the simulations, it is unfortunately quite noisy. Aside from the problem noted above of large atomic-level force fluctuations in general, here the procedure used to generate the motion exacerbates the problem. The atoms at the ends of the filament are attached to moving tether sites by stiff springs, whose force is very sensitive to small atomic displacements.

In the constant-velocity simulations the result is simple – the pulling force is roughly constant in time, fluctuating about a value which is approximately linearly proportional to the pulling velocity. At the three velocities studied, 0.05, 0.15 and  $0.5\sigma/\tau$ , the force per pulled monomer is measured to be  $2.72 \pm 0.16$ ,  $7.31 \pm 0.24$  and  $24.9 \pm 0.25\epsilon/\sigma$ , respectively. (Typical values of the instantaneous force on a monomer at this density and temperature are  $O(1-10)$  in this unit, while its time averaged values over a  $100\tau$  interval are an order of magnitude smaller.) One can rationalize the time-constancy of the force by arguing that in this case the molecules are moving past each other with a roughly fixed value of relative velocity, and since the material is a viscous liquid in a low Reynolds number flow, there is a constant drag force on each molecule.

In contrast, in the constant strain rate cases there is a non-trivial time variation. For example, as shown in Fig. 15 for the lowest rate  $\dot{\epsilon}_0 = 0.001\tau^{-1}$ , the tether force jumps to a finite value once the force is applied, then increases with time until about  $1750\tau$ . After a sharp drop, the force again increases until rupture. Referring to Fig. 10, after this transition time the right and left sides of the filament are approximately translating without a significant shape change, while the central region thins down to nothing. The early increase can then be associated with strain hardening [3,9] and the shape deformation of the entire liquid filament; the sharp drop with relaxation of stress after some internal readjustment and formation of the central neck; the second increase with the strain hardening of the central thinner region; and the final drop-off with rupture. At the next highest strain value,  $0.004\tau^{-1}$ , the numerical values of the tether force are comparable, and the tether force shows a similar variation, with a corresponding drop at about  $600\tau$ , the time at which (see Fig. 13) the central region of the filament halts and ceases to change its shape while the regions to either side continue to elongate. At still highest strain rates there is no obvious pattern to the tether force evolution; the fragmentation of the regions near the tethers makes it difficult to identify simple mechanisms.

We can also compute the forces in the interior of the filament, and in Fig. 16 we show an example of the force in the axial direction in the  $\dot{\epsilon}_0 = 0.001$  constant strain rate simulation at time  $2150\tau$ , averaged over a  $100\tau$  time interval and a  $6\sigma$  spatial interval along the axis. The force on the end regions containing the tethered monomer shows large spatial and temporal fluctuations for the reasons given at the beginning of this Section, and these two regions have been suppressed in this plot. Aside from the fluctuations, the trend is a roughly-linear ramp with positive (negative) values corresponding to the halves of the filament moving to the right (left). As a function of time, the fluctuations shift around apparently randomly, and the height of the ramp is roughly constant in time. At higher strain rates, the analogous plot is again a fluctuating quasi-linear ramp in its central region, but shows rapid spatial fluctuations near the ends, corresponding to molecules being pulled out there. In contrast, in the constant-velocity simulations there is always a linear ramp as a function of  $z$ , and furthermore, at different pulling speeds the ramp height is roughly linear in velocity.

## VI. CONCLUSIONS

We have discussed the results of molecular simulations of a liquid filament of model polymer melt stretched to the point of rupture. These model systems are composed of non-breakable, freely-jointed, entangled chains, and the rupture process typically involves ductile failure of some sort. Here we observed these filaments stretch into a very non-uniform shape, with one or more thin necked regions, and then fail when one of the necks simply attenuates down to nothing. More precisely, during the stretching process the thinning neck regions are populated with well-extended chain molecules lying roughly parallel to the extension axis, which are drawn past each other to one side or the other by their respective interacting neighbors. Eventually the filament is held together by only a few such adjacent elongated chains, and splits once these slide past each other. In continuum terms, the neck thins under a combination of mass transfer due to outflow and (Rayleigh) capillary instability. In analogous earlier simulations in systems of melts or solutions based on shorter length molecules (up to 20 monomers), presumably unentangled, a more familiar form of ductile fracture was observed in which a neck several molecules in thickness separated into two pieces [9]. In

that case, a model solution was able to attain the longest lengths prior to breakup, and there one could see that the fully-extended longer molecules acted as a backbone which stiffened the filament, and breakage occurred when the filament was extended to the point that these backbone molecules were no longer in contact with each other.

In term of the classification of failure zones by Malkus and Petrie [6], the constant velocity and lowest-rate constant strain runs are in the “flow zone”, where viscous deformation can proceed indefinitely provided there is enough liquid. The two runs at higher constant strain appear to have “glassy states”, at least near the tethers where rupture occurs.

The filament shapes observed here seem unusually irregular compared to those studied elsewhere, and in no case do we observe a long neck of nearly constant diameter. Note however, that these simulations begin with a liquid sample whose diameter is already in the nanometer range, and so these results should at best be compared to the last, usually poorly-quantified stages of typical laboratory studies. The surface irregularities and fluctuations are, however, quite characteristic of molecular simulations of moving microscopic liquid bodies with free surfaces [7,22]. In consequence of these fluctuations, the measured continuum fields show sufficiently large statistical fluctuations as to be non-trivial to understand even qualitatively. Even microscopic measurements which do yield a smooth result, such as the variation of minimum filament radius with time, are not in agreement with continuum calculations. The molecular level information is likewise fluctuating, but does seem to be readily interpretable at this scale.

A further issue in comparing these results to laboratory measurements is the pulling speed involved. Although the standard dimensionless groups characterizing these flows, the Reynolds, Deborah and capillary numbers, are similar to those considered elsewhere, there is quite a difference in velocities. In typical liquid flows the drift or peculiar velocity is a small fraction of the thermal velocity of the monomers, but here, particularly in the late stages of the constant strain simulations, the tether velocity approaches the thermal velocity,  $O(1/\sigma/\tau)$ . The severe fragmentation of the end regions of the filament is presumably one aspect of this high speed, but a second is that surface tension effects which would ordinarily smooth a free surface may not have time to act.

#### ACKNOWLEDGMENTS

We thank the NASA Office of Physical and Biological Sciences for financial support, and the NASA Advanced Supercomputing Division at the Ames Research Center, and NPACI at the San Diego Supercomputer Center for providing computational resources.

---

- [1] R. I. Tanner, *Engineering Rheology*, 2nd ed. (Oxford, New York, 2000); N. G. McCrum, C. P. Buckley and C. B. Bucknall, *Principles of Polymer Engineering*, 2nd ed. (Oxford, New York, 1997).
- [2] R. B. Bird, C. F. Curtiss, R. C. Armstrong and O. Hassager, *Dynamics of Polymeric Liquids*, 2nd ed., 2 vols. (Wiley, New York, 1987).
- [3] G. H. McKinley and T. Sridhar, Annu. Rev. Fluid Mech. **34**, 375 (2002).
- [4] J. Eggers, Rev. Mod. Phys. **69**, 865 (1997).
- [5] C.-M. Ho and Y.-C. Tai, Annu. Rev. Fluid Mech. **30**, 579 (1998); G. E. Karniadakis and A. Beskok, *Micro Flows: Fundamentals and Simulation* (Springer, New York, 2002).
- [6] A recent discussion with extensive references is A. Ya. Malkin and C. J. S. Petrie, J. Rheol. **41**, 1 (1997).
- [7] J. Koplik and J. R. Banavar, Phys. Fluids **A5**, 521 (1993).
- [8] J. Koplik, S. Pal and J. R. Banavar, Phys. Rev. E **65**, 021504 (2002).
- [9] B. Busic, J. Koplik and J. R. Banavar, “Molecular dynamics simulations of liquid-bridge extensional flows,” submitted to J. Non-Newtonian Fluid Mech. (2002).
- [10] M. Cheon, I. Chang, J. Koplik and J. R. Banavar, Europhys. Lett. **58**, 215 (2002).
- [11] M. P. Allen and D. J. Tildesley, *Computer Simulation of Liquids* (Clarendon Press, Oxford, 1987).
- [12] J. Koplik and J. R. Banavar, Annu. Rev. Fluid Mech. **27**, 257 (1995).
- [13] K. Kremer and G. S. Grest, J. Chem. Phys. **92**, 5057 (1990). This paper deduced an entanglement length of 35, while more recent work [M. Putz, K. Kremer and G. S. Grest, Europhys. Lett. **49**, 735 (2000)] gives a revised estimate of 70.
- [14] K. Binder, ed., *Monte Carlo and Molecular Dynamics Simulations in Polymer Science* (Oxford, New York, 1995).
- [15] M. Kröger, W. Loose and S. Hess, J. Rheol. **37**, 1057 (1993).
- [16] J. S. Rowlinson and B. Widom, *Molecular Theory of Capillarity* (Oxford University Press, Oxford, 1982).
- [17] S. Nosé, Mol. Phys. **52**, 255 (1984); W. G. Hoover, Phys. Rev. A **31**, 1695 (1985).
- [18] S. B. Smith, L. Finzi and C. Bustamante, Science **258**, 1122 (1992).
- [19] I. Cohen and S. R. Nagle, Phys. Fluids **13**, 3533 (2001).

- [20] A. U. Chen, P. K. Notz and O. A. Basaran, Phys. Rev. Lett. **88**, 174501 (2002).
- [21] M. Kröger, C. Luap and R. Muller, Macromolecules **30**, 526 (1997).
- [22] M. Moesler and U. Landman, Science **289**, 1165 (2000).

|                             | Constant velocity |      |      | Constant strain rate |       |      |
|-----------------------------|-------------------|------|------|----------------------|-------|------|
| $v_0$ or $\dot{\epsilon}_0$ | 0.05              | 0.15 | 0.5  | 0.001                | 0.004 | 0.01 |
| length                      | 432               | 694  | 1080 | 701                  | 1594  | 959  |
| time                        | 3520              | 2045 | 1000 | 2250                 | 763   | 263  |

**Table I.** Final length and time to rupture (MD units).

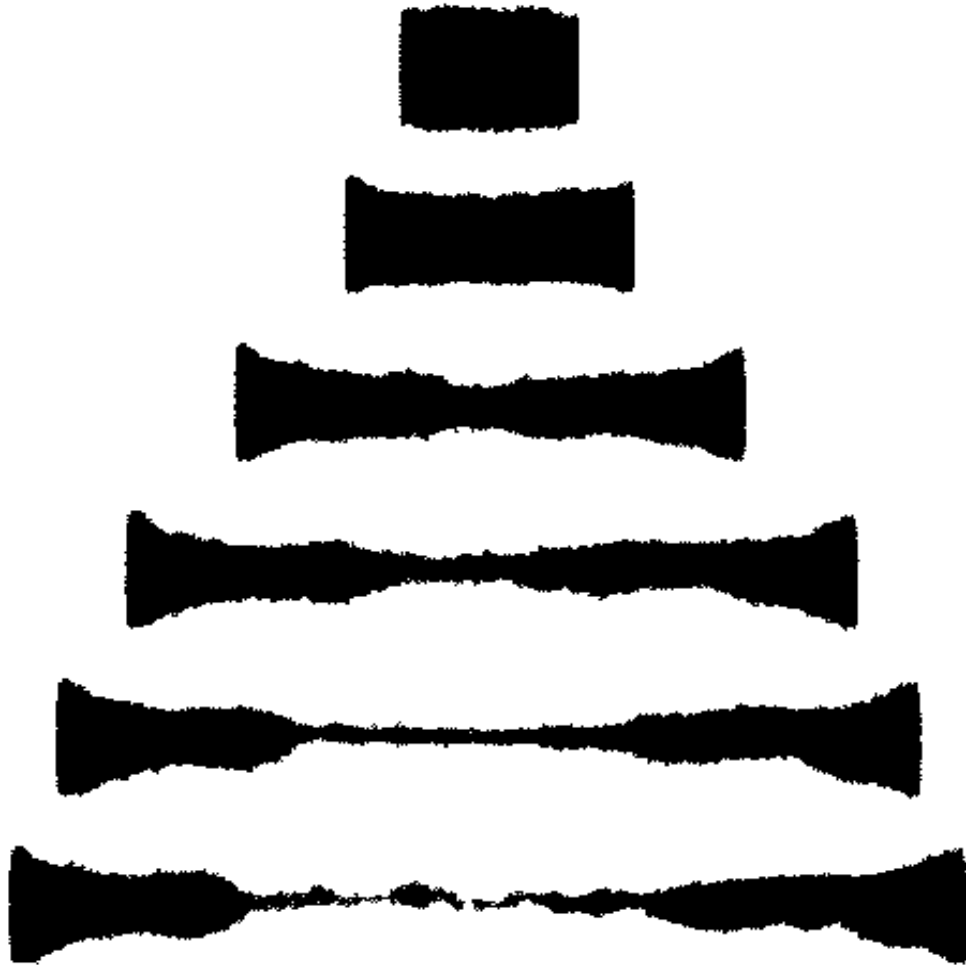


FIG. 1. Sequence of filament shapes in a constant velocity deformation at pulling speed  $v_0 = 0.05\sigma/\tau$ , at times 0, 500, 1500, 2500, 3100 and  $3520\tau$  (top to bottom).

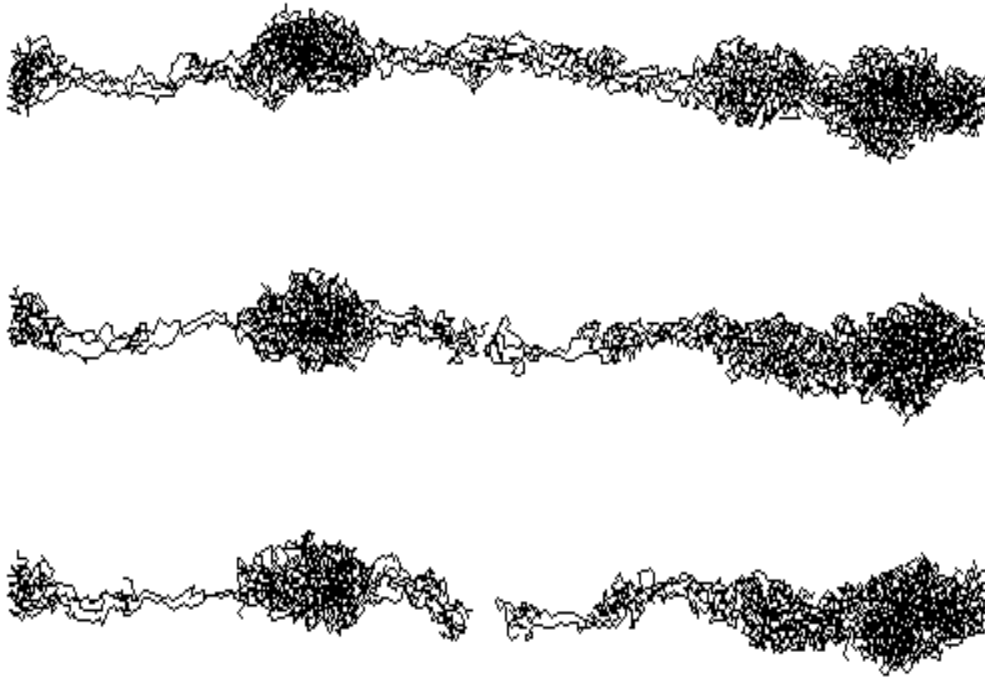


FIG. 2. Rupture region in the constant velocity deformation of Fig. 1, at times  $3475$ ,  $3515$  and  $3520\tau$  (top to bottom).

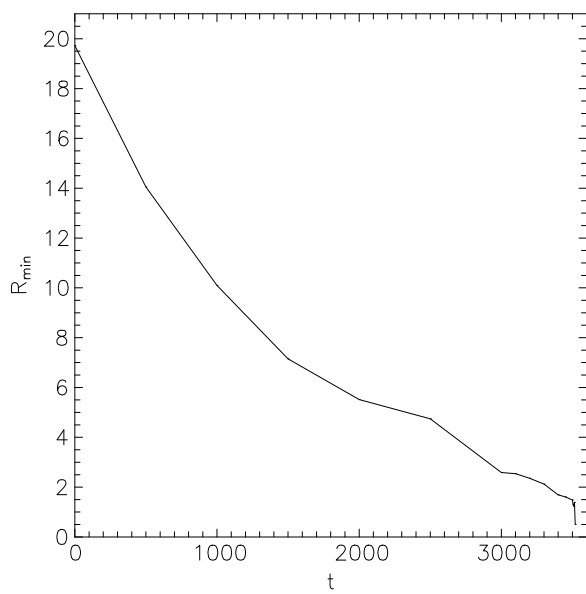


FIG. 3. Minimum radius *vs.* time in the constant velocity deformation of Fig. 1.

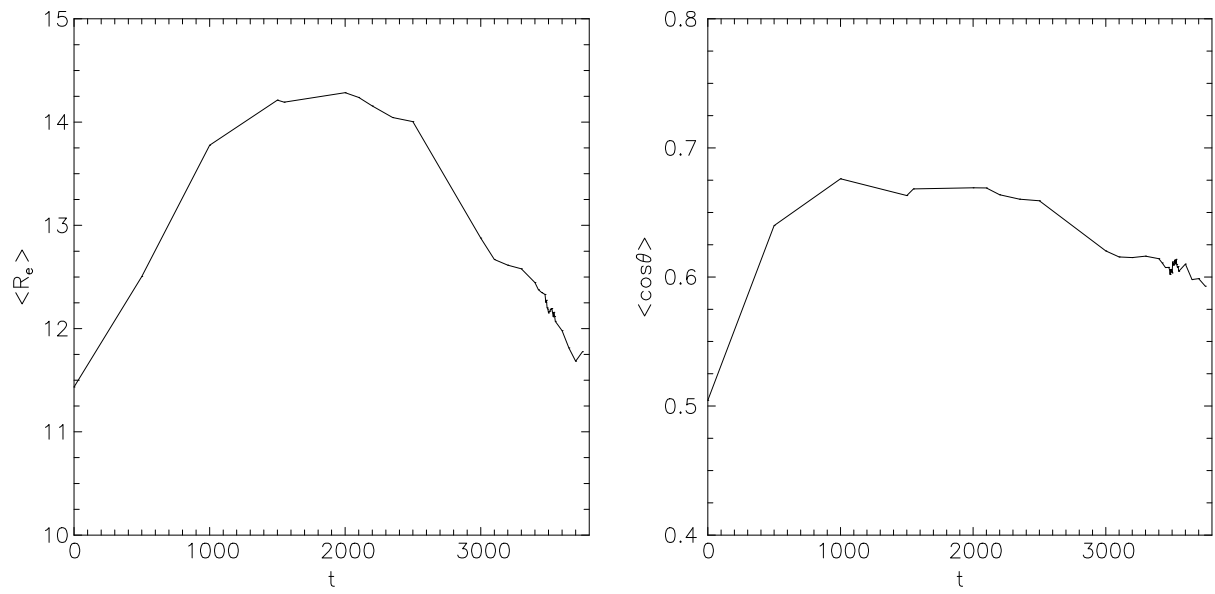


FIG. 4. Mean molecular end-to-end length and orientation angle *vs.* time in the constant velocity deformation of Fig. 1.

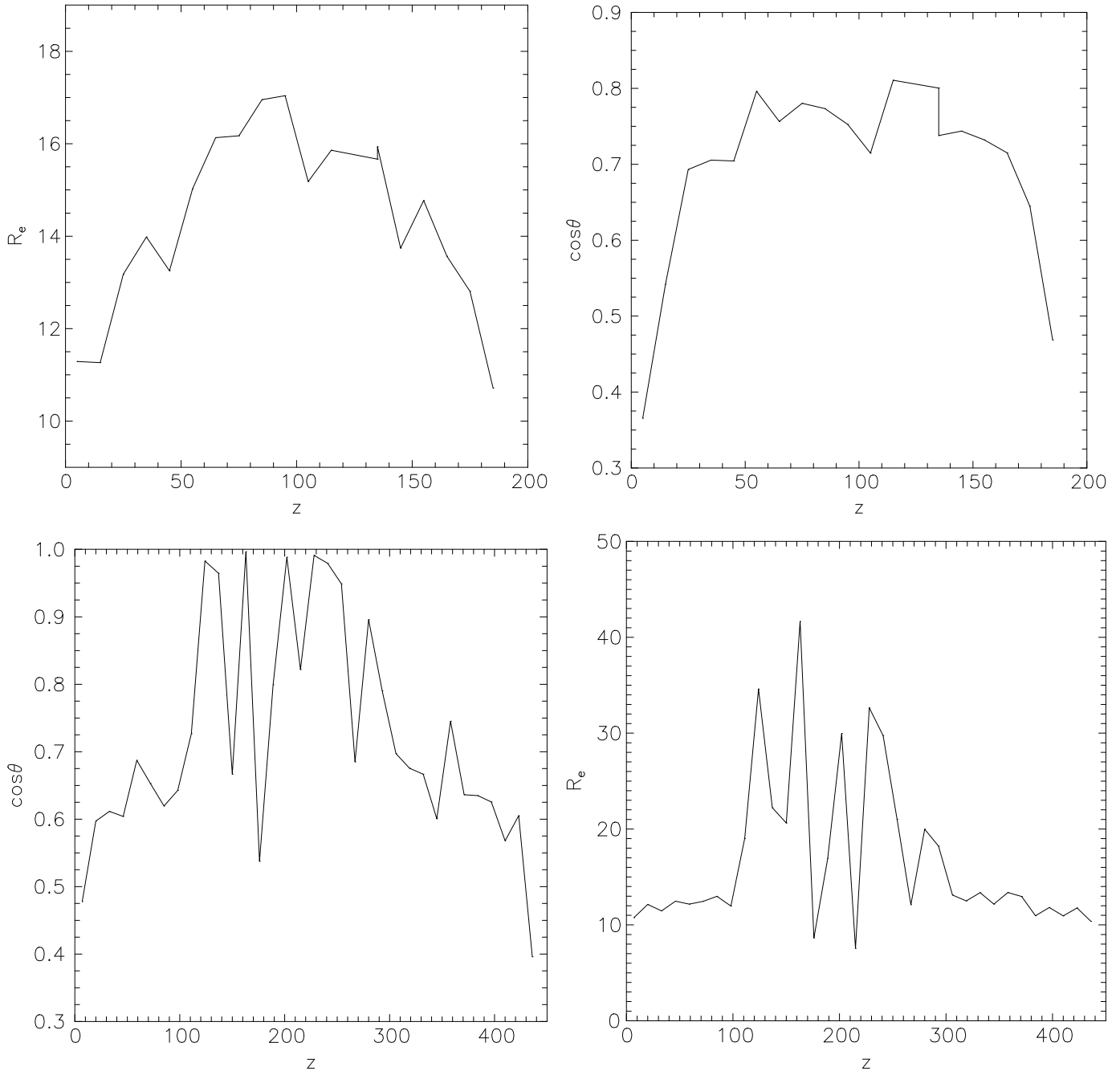


FIG. 5. Molecular length and molecular orientation *vs.* axial position, in the constant velocity deformation of Fig. 1. (top) at time  $1000\tau$ , (bottom) at time  $3500\tau$ .

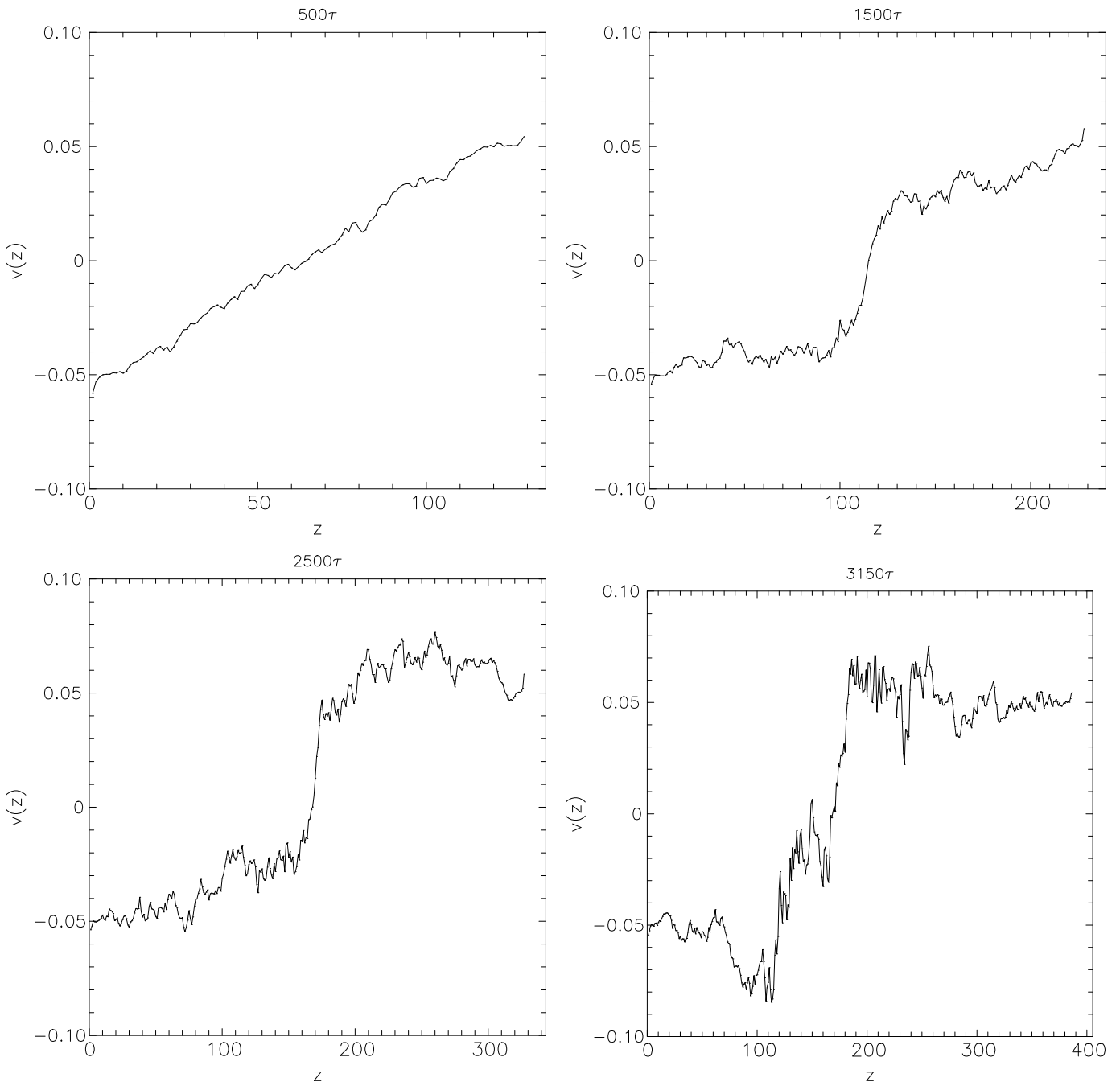


FIG. 6. Velocity *vs.* axial position in the constant velocity deformation of Fig. 1 at the times indicated. Each curve represents a  $50\tau$  time average.

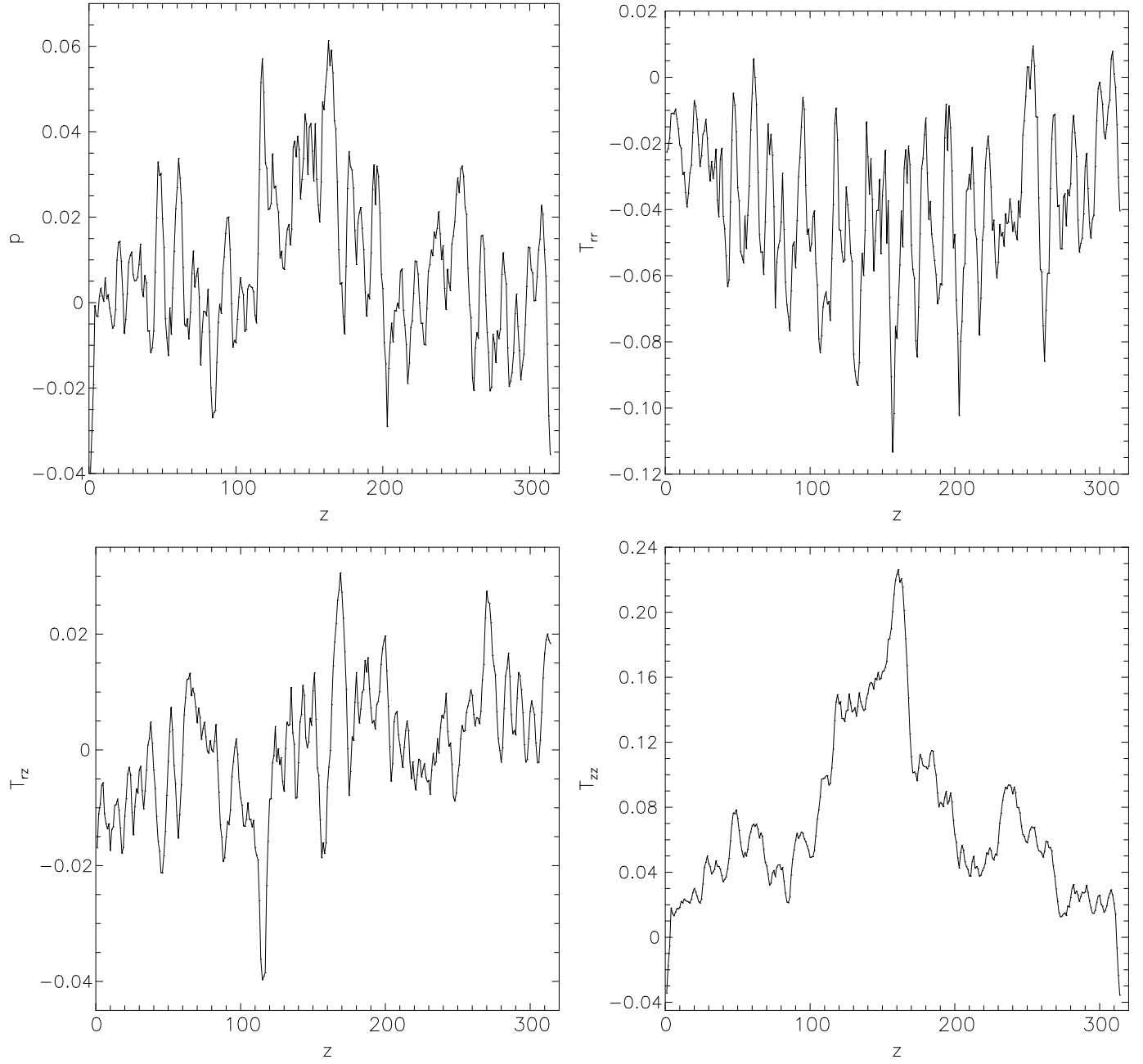


FIG. 7. Stress tensor components *vs.* axial position in the constant velocity deformation of Fig. 1 at time  $2500\tau$ . Clockwise from upper left: pressure ( $p$ ), radial ( $rr$ ), axial ( $zz$ ), and shear ( $rz$ ) stress.

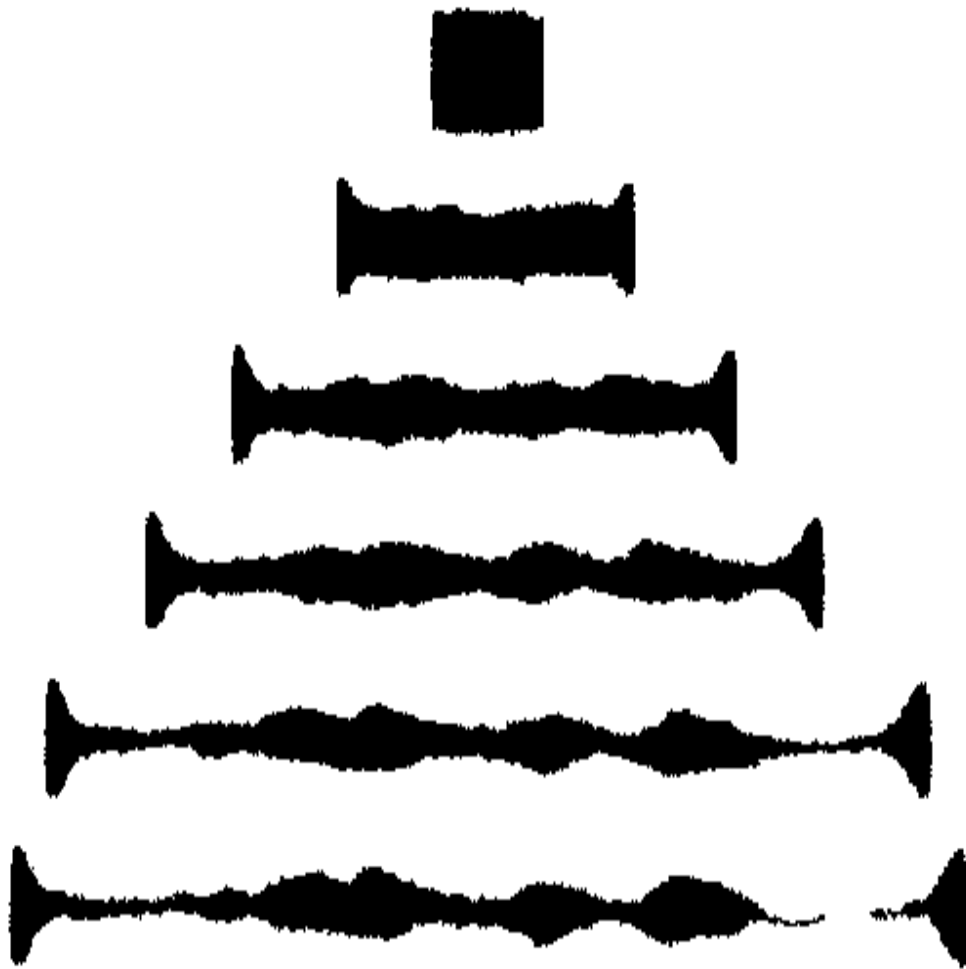


FIG. 8. Sequence of filament shapes in a constant velocity deformation at pulling speed  $v_0 = 0.15\sigma/\tau$ , at times 0, 450, 950, 1770, 1870 and  $2045\tau$ .

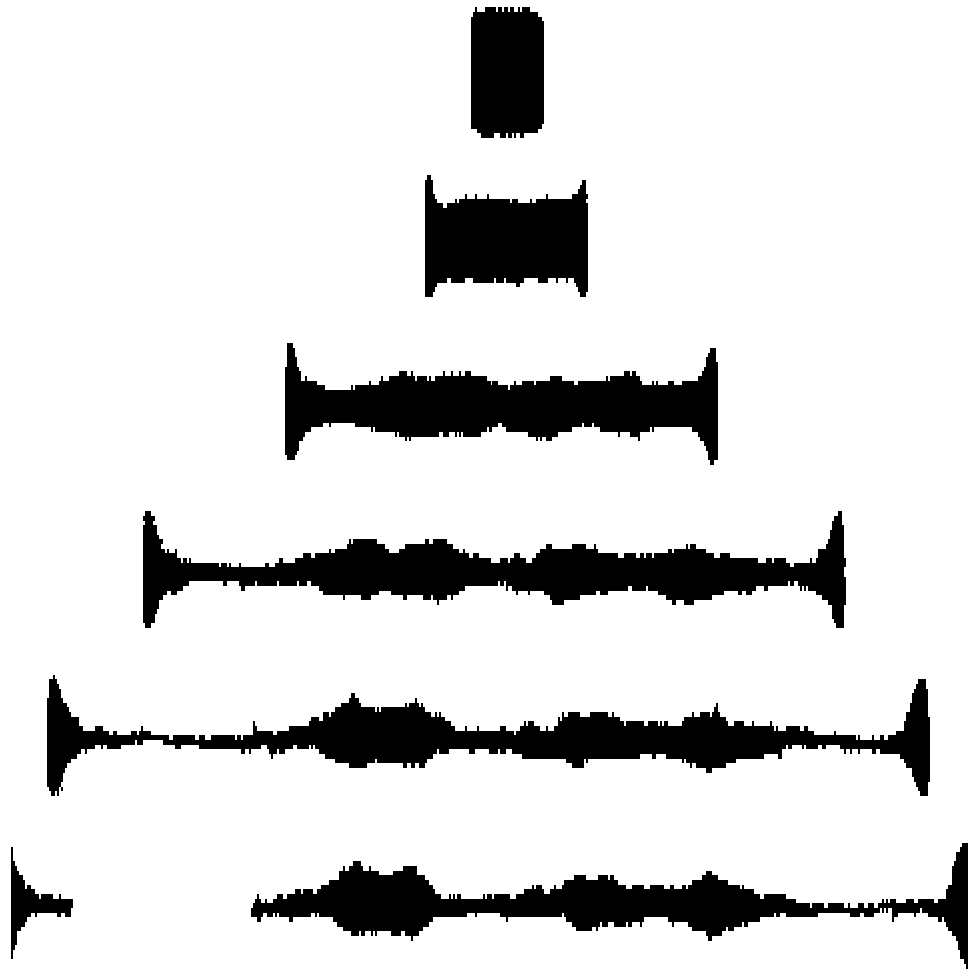


FIG. 9. Sequence of filament shapes in a constant velocity deformation at pulling speed  $v_0 = 0.5\sigma/\tau$ , at times 0, 100, 400, 700, 900 and  $1000\tau$ .

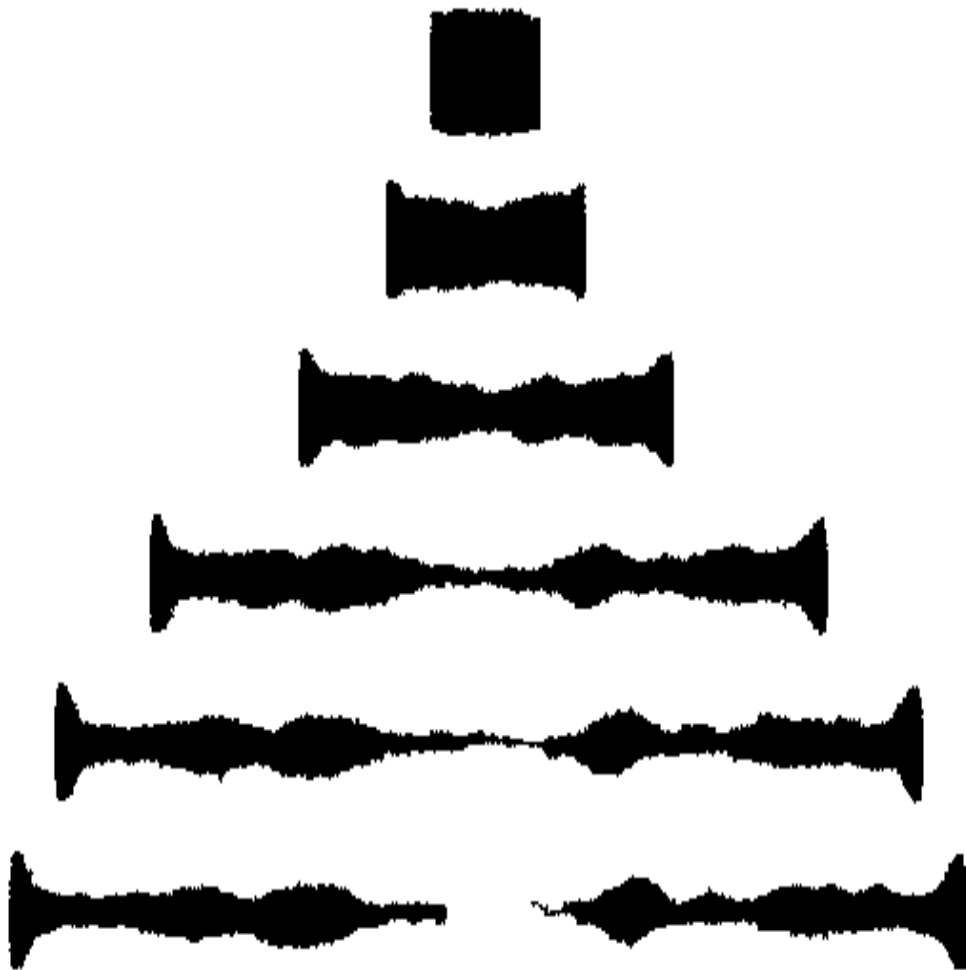


FIG. 10. Sequence of filament shapes in a constant strain rate deformation at  $\dot{\epsilon}_0 = 0.001\tau^{-1}$ , at times 0, 650, 1300, 1950, 2150 and  $2250\tau$ .

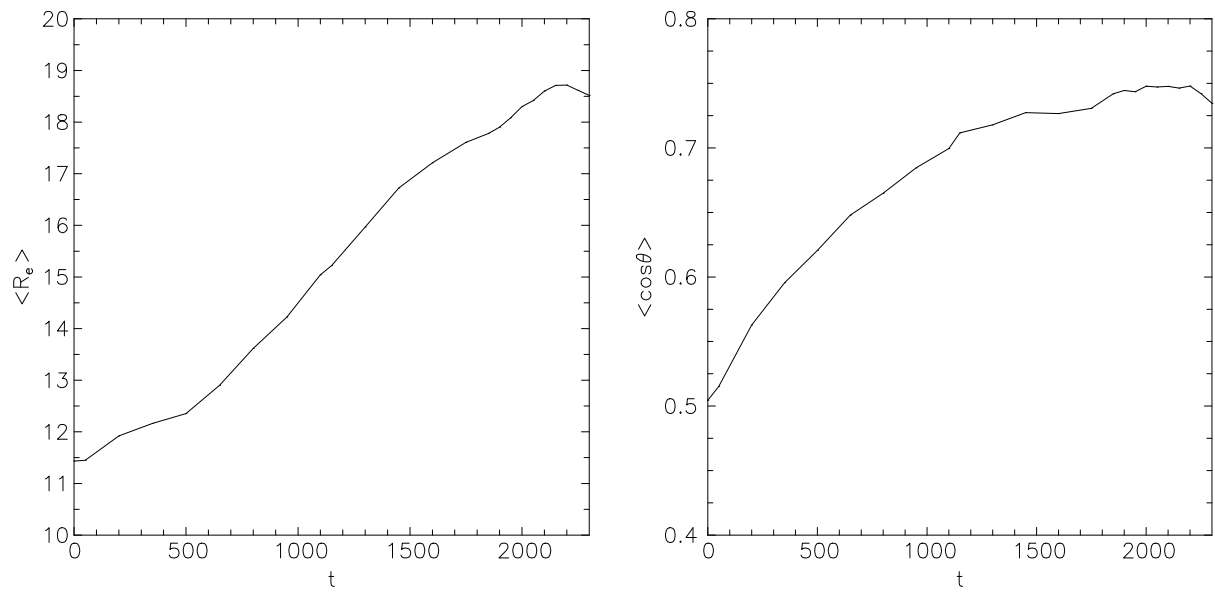


FIG. 11. Mean molecular end-to-end length and orientation angle *vs.* time in the constant strain deformation of Fig. 10.

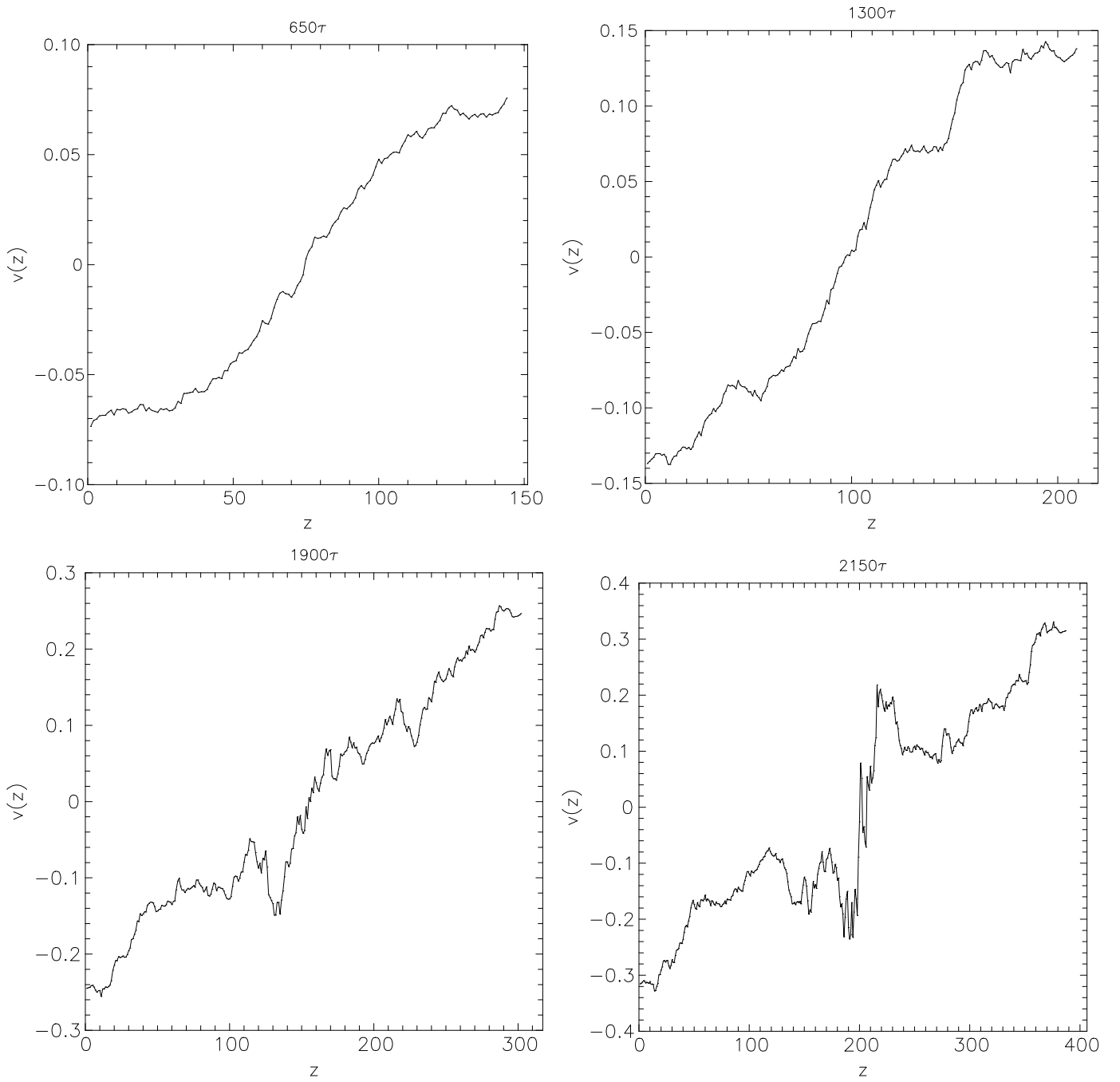


FIG. 12. Velocity *vs.* axial position in the constant velocity deformation of Fig. 10 at the times indicated. Each curve represents a  $50\tau$  time average.

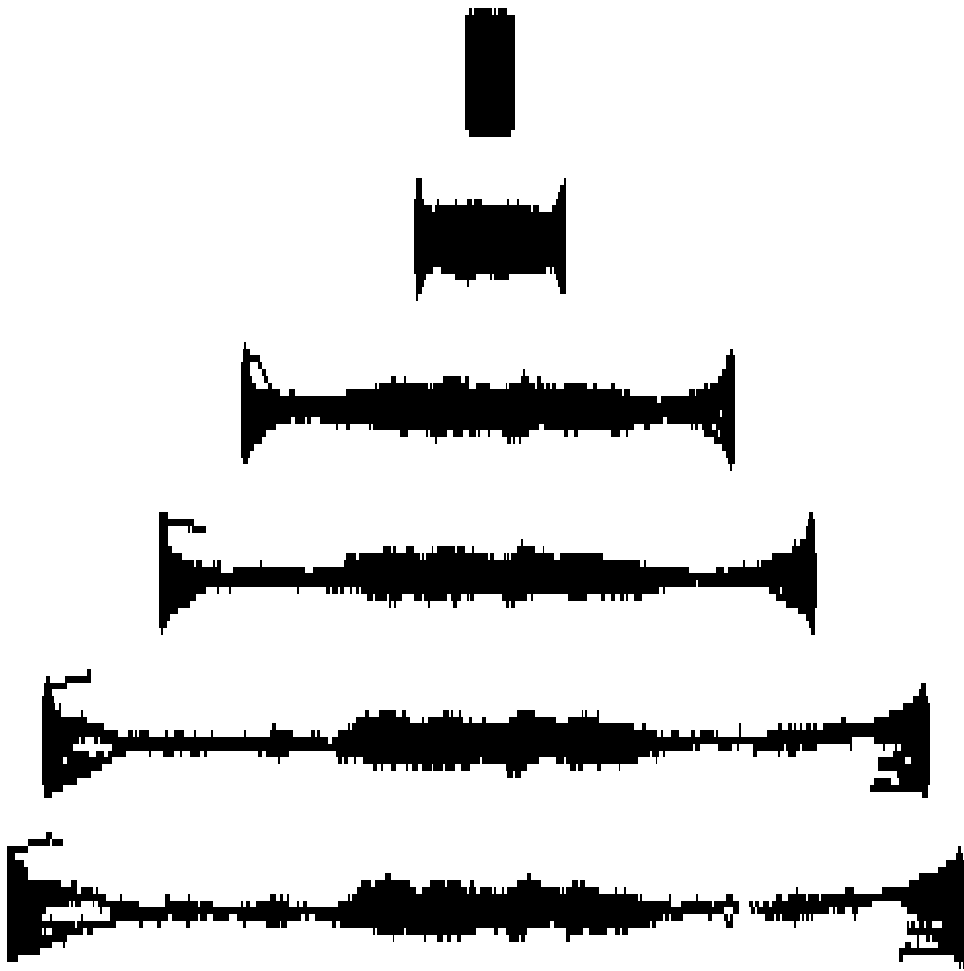


FIG. 13. Sequence of filament shapes in a constant strain rate deformation at  $\dot{\epsilon}_0 = 0.004\tau^{-1}$ , at times 0, 295, 595, 668, 743 and  $763\tau$ .

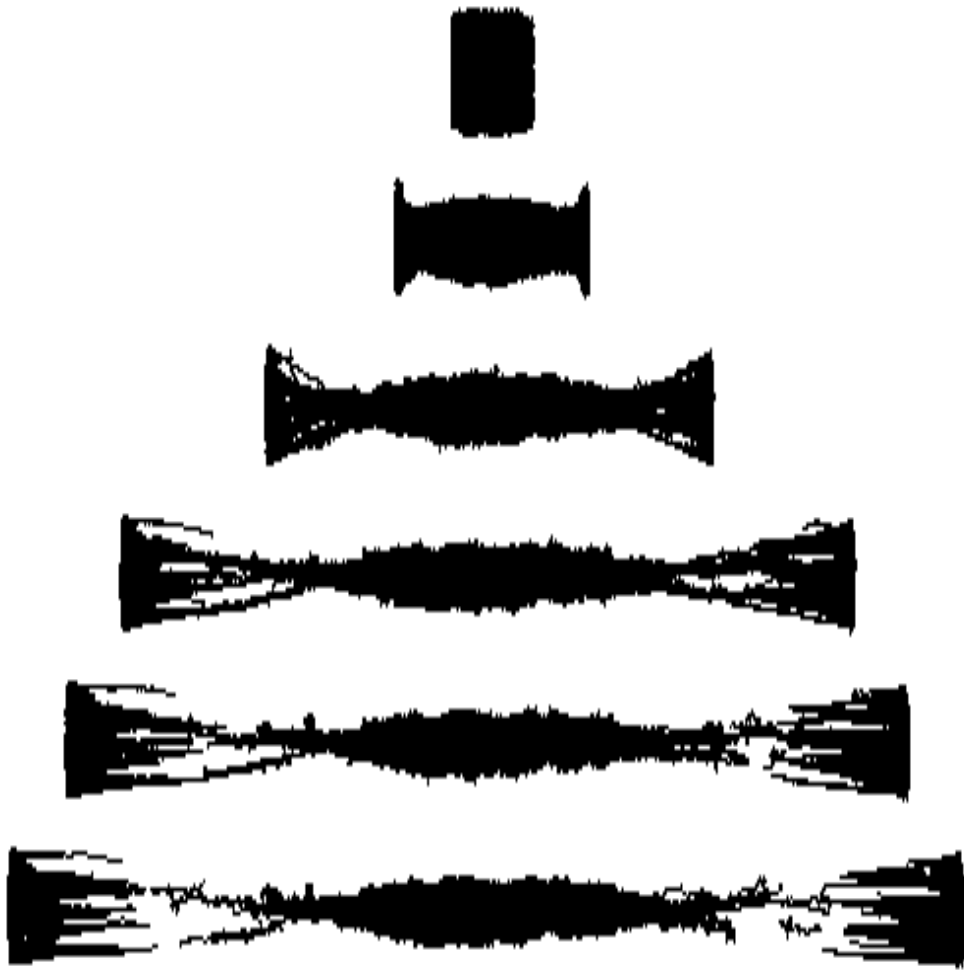


FIG. 14. Sequence of filament shapes in a constant strain rate deformation at  $\dot{\epsilon}_0 = 0.01\tau^{-1}$ , at times 0, 90, 175, 225, 240 and  $253\tau$ .

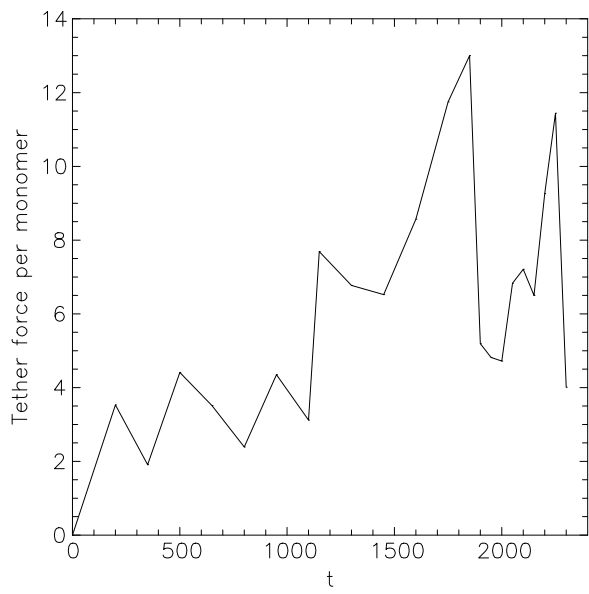


FIG. 15. Variation of the tether force with time, in the simulation shown in Fig. 10.

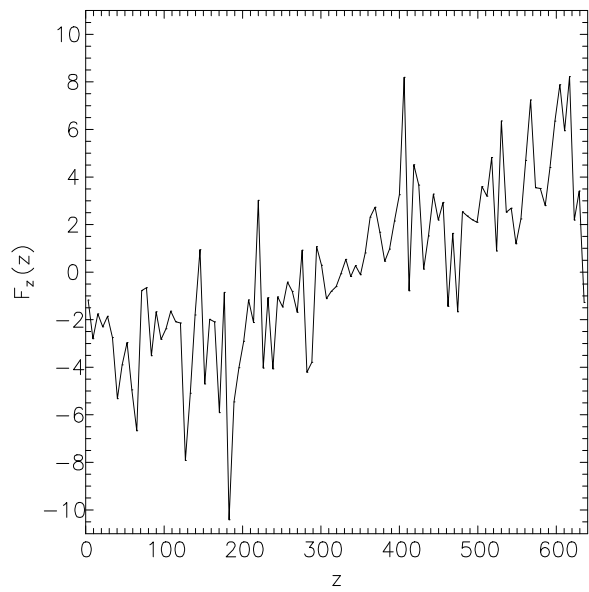


FIG. 16. Axial force as a function of axial position in the filament shown in Fig. 10, at time  $2150\tau$ .